Title	Multiscale fluid-structure interaction modelling to determine the mechanical stimulation of bone cells in a tissue engineered scaffold
Author(s)	Zhao, Feihu; Vaughan, Ted J.; McNamara, Laoise M.
Publication Date	2015-04
Publication Information	Zhao, Feihu, Vaughan, Ted J., & Mcnamara, Laoise M. (2015). Multiscale fluid–structure interaction modelling to determine the mechanical stimulation of bone cells in a tissue engineered scaffold. Biomechanics and Modeling in Mechanobiology, 14(2), 231-243. doi: 10.1007/s10237-014-0599-z
Link to publisher's version	http://dx.doi.org/10.1007/s10237-014-0599-z
Item record	http://hdl.handle.net/10379/6225
DOI	http://dx.doi.org/10.1007/s10237-014-0599-z

Multiscale fluid structure interaction modelling to determine the mechanical stimulation of bone cells in a tissue engineered scaffold

Feihu Zhao, Ted J. Vaughan, Laoise M. Mcnamara

Biomechanics Research Centre (BMEC), Biomedical Engineering, College of Engineering and Informatics, National University of Ireland, Galway, Ireland

Corresponding author:

Laoise M. McNamara

Contact information:

Biomechanics Research Centre (BMEC), Biomedical Engineering, College of Engineering and Informatics, National University of Ireland, Galway, Ireland

Tel.: +353-91-492251;

Fax: +353-91-563991;

E-mail: laoise.mcnamara@nuigalway.ie

Abstract

Recent studies have shown that mechanical stimulation, by means of flow perfusion and mechanical compression (or stretching) enhances osteogenic differentiation of MSCs and bone cells within biomaterial scaffolds *in vitro*. However the precise mechanisms by which such stimulation enhances bone regeneration is not yet fully understood. Previous computational studies have sought to charaterise the mechanical stimulation on cells within biomaterial scaffolds using either computational fluid dynamics (CFD) or finite element (FE) approaches. However the physical environment within a scaffold under perfusion is extremely complex, and requires a multiscale and multiphysics approach to study the mechanical stimulation of cells. In this study, we seek to determine the mechanical stimulation of osteoblasts seeded in a biomaterial scaffold under flow perfusion and mechanical compression using multiscale modelling by two-way fluid structure interaction (FSI) and FE approaches. The mechanical stimulation, in terms of wall shear stress (WSS) and strain in osteoblasts, is quantified at different locations within the scaffold for cells of different attachment morphologies (attached, bridged). The results show that 75.4% of scaffold surface has a WSS of 0.1mPa - 10mPa, which indicates the likelihood of bone cell differentiation at these locations. For attached and bridged osteoblasts, the maximum strains are 397με and 177,200με, respectively. Additionally, the results from mechanical compression show that attached cells are more stimulated (maximum strain=22,600με) than bridged cells (maximum strain=10,000με). Such information is important for understanding the biological response of osteoblasts under *in vitro* stimulation. Finally, a combination of perfusion and compression of a TE scaffold is suggest for osteogenic differentiation.

Keywords Fluid-structure interaction · Multiscale modelling · Osteoblast · Tissue engineered scaffold

1. Introduction

Tissue engineering and regenerative medicine are promising strategies for replacing defective bone tissue and reconstructing bone defects to treat bone diseases and overcome the limitations of traditional bone graft replacement techniques, which include restricted bone availability, the requirement for additional invasive surgery and suffering of patients. Current bone tissue engineering (TE) approaches involve growing mesenchymal stem cells (MSCs) under *in vitro* conditions on either natural or synthetic biomaterial scaffolds. Using such approaches, it has been shown that MSCs can differentiate along the osteogenic pathway in the presence of various biochemical factors and various biomaterial scaffolds, for example PLGA and collagen, and can elicit tissue differentiation *in vitro* that is indicative of bone formation (Lupu-Haber et al. 2013; Li et al. 2013; Park et al. 2012; Xie et al. 2013; Vozzi et al. 2013). However, existing TE approaches have not been able to regenerate tissue *in vitro* that can be used clinically to replace degenerated bone, support loading and enhance the growth and differentiation of new bone tissue *in vivo*. Particular limitations of current approaches are poor nutrient transport in biomaterial scaffolds, resulting in death of cells in scaffold cores, failure of the regenerated tissue to integrate with the host tissue and, most importantly, the tissue produced is not adequately stiff to fulfill load bearing functions in the body. Recent studies have shown that mechanical stimulation enhances bone tissue regeneration *in vitro* to a certain extent (Sittichockechaiwut et al. 2009; Jaasma et al. 2008; Goldstein et al. 2001). In particular, it has been shown that osteogenic differentiation, as indicated by ALP, COX_2 and PGE_2 expression (Thompson et al. 2010; Keogh et al. 2011; Liu et al. 2012), is enhanced when bone cells are exposed to the fluid flow, compared to static culture (Jaasma et al. 2008; Goldstein et al. 2001; Li et al. 2009). Such changes could be related to the enhanced nutrient transport or mechanical stimulation of the cells within the scaffolds, but the precise nature of such changes is not yet known. In particular osteoblasts are sensitive to flow-induced shear stress, as has been demonstrated by *in vitro* studies of osteogenic responses by osteoblasts exposed to fluid shear stresses (Owan et al. 1997; You et al. 2000). Osteocytes are also sensitive to fluid shear stress and can transduce these mechanical stimuli into biochemical responses (Bacabac et al. 2004; Klein-Nulend et al. 1995), and indeed are thought to be

the most sensitive bone cell type to mechanical stimulation (Klein-Nulend et al. 1995; Westbroek et al. 2000). Therefore, the quantification of mechanical stimulation on bone cells, in particular flow-induced shear stress, is necessary to inform future in vitro bone tissue regeneration strategies.

Tissue differentiation within biomaterial scaffolds is heterogeneous, due to variations in scaffold architecture and restrictions on fluid flow across different regions of the scaffold (Lyons et al. 2010; Samavedi et al. 2012; Kim et al. 2010). Computational modelling has been applied to predict the mechanical stimulation experienced within tissue engineered scaffolds under flow perfusion or mechanical compression/stretching *in vitro* (Byrne et al. 2007; Stops et al. 2008; Stops et al. 2010; Olivares et al. 2009; Milan et al. 2009; Ryan et al. 2009; Jungreuthmayer et al. 2009; McCoy et al. 2012). In general, these models have simulated the mechanical environment within biomaterial scaffolds using either finite element (FE) approaches or computational fluid dynamics (CFD). FE models have been applied to predict the biophysical stimuli created within idealised and μ-CT derived models of collagen-GAG scaffolds. For instance, Byrne et al. (2007) employed FE modelling, in combination with an adaptive mechanoregulation algorithm, to investigate bone tissue differentiation within an idealised scaffold under compression. Stops et al. (2008, 2010) used an FE approach to study the mechanical stimuli experienced by cells in different regions of a realistic collagen-GAG scaffold under tensile stretch and compressive loading. The results showed a wide range of mechanical stimuli experienced by cells in different regions in the scaffolds due to a regional dependence of architectural and mechanical properties of the scaffold caused by the manufacturing process. In addition, CFD models have been used to predict the wall shear stress (WSS) along the scaffold surface arising under fluid flow through the scaffold (Olivares et al. 2009; Milan et al. 2009; Ryan et al. 2009). Both realistic and idealised scaffolds in these studies were assumed as rigid and cell-free, exposed to the fluid flow. The results showed that not only the input flow rate, but also the scaffold architecture and porosity had an influence on the mechanical stimuli (WSS) on the scaffold surfaces. However, these studies excluded the cells, which are composed of an elastic cell membrane that deforms in response to the fluid flow imposed by perfusion through the scaffold. A recent CFD-elastostatics approach has been applied to model the geometry of the scaffolds from μ-CT scanned data and to include cells attached to the biomaterial scaffold (Jungreuthmayer et al. 2009; McCoy et al.

2012). These models represented the geometrical features of the *in vitro* environment and were applied to predict the WSS on cells and the resulting deformation of cells seeded within a flow perfusion bioreactor. These studies identified that cells that were bridged between two struts experienced much higher deformation than cells that were just attached to a single strut and therefore highlighted the importance of the scaffold pore size in determining the nature of cell attachment. However, these studies were carried out using a one-way Fluid-Structure Interaction (FSI) approach and did not consider the influence of cellular deformation on the surrounding fluid flow.

In recent studies, advanced two-way fluid structure interaction (FSI) methods have been applied to model the complex interaction between soft cells and tissues and extracellular fluid flow (Birmingham et al. 2013; Vaughan et al. 2013, Verbruggen et al. 2013). This approach allows deformable structures and resulting fluid flow fields to be predicted. By using the two-way FSI and multilevel methodologies, Vaughan et al. (2013) predicted with high resolution flow fields and cellular deformation, and revealed the influence of WSS and fluid pressure on the bone cells that were cultured in a parallel-plate flow chamber system. Verbruggen et al. (2013) applied a two-way FSI to precisely obtain the WSS and strain of the osteocytes *in vivo* environment. However, as yet these fully-coupled, high resolution techniques have not been applied to examine the 3D culture environment of bone cells in a TE scaffold.

The objective of this study is to apply two-way FSI and FE approaches to investigate the nature of the mechanical stimulation experienced by individual osteoblasts seeded on a biomaterial scaffold and exposed to flow perfusion and mechanical compression. A multilevel methodology is developed whereby a global CFD model is used to characterise the mechanical stresses within the scaffold under flow perfusion, while a local FSI model, informed by the results of the global model, is used to characterise the nature of the deformation experienced by osteoblasts attached within the scaffold. The cell-level models include the internal nucleus and cytoplasm, and the nature of mechanical stimulation on osteoblasts at different locations within the scaffold are analysed. Furthermore, the stimulation on osteoblasts due to mechanical compression is investigated using a FE model. Such results are significant in order to precisely describe the mechanical stimulation of osteoblasts at different locations in the scaffold.

2. Materials and Methods

For the perfusion system, the model was formulated at two separate length scales as illustrated in Fig. 1. At the global level, we developed a CFD model of an idealised scaffold with the hexagonal architecture (Fig. 2(a)) to predict local shear stress stimulation within the scaffold under typical flow perfusion regimes used *in vitro*. These results were used to define the boundary conditions for the sub-scaffold (cellular level) FSI model, providing a framework to relate scaffold level stimulation to local cellular deformation. This approach is described in further detail below. For the mechanical compression, the strains in osteoblasts were determined by a FE method as described in Section 2.3.

2.1 Global computational fluid dynamics model

To define the boundary conditions for the sub-scaffold (cellular level) model, a computational fluid dynamics global model (CFD) model of the scaffold was developed using ANSYS CFX (ANSYS, Inc., US). Based on the studies by Olivares et al. (2009), the scaffold had a diameter of 8 mm and a regular hexagonal architecture, a porosity of 55% and a pore size l_1=85 μm (width), l_2=179.5 μm (length) (see Fig. 2(a, b)). The central region of the scaffold (0.8 mm diameter and 4 mm length) was modelled as a series of repeating units in both the radial and longitudinal directions (8 mm diameter and 4 mm length). The model was meshed with 1,823,000 tetrahedral elements to resolve pressure and velocity fields inside the scaffold under steady-state conditions.

The scaffold was fabricated from poly(D,L-lactide) (PDLLA) material, which had a Young's modulus and Poisson's ratio of 3.3GPa and 0.3, respectively (Olivares et al. 2009). As the Young's modulus of the scaffold material was high, the influence of the fluid on the solid scaffold was neglected in the global CFD model. The perfusion media, Dulbecco's Modified Eagle Medium (DMEM) was modelled as a Newtonian fluid with a dynamic viscosity of μ = 1.45 mPa and a density of ρ = 1000 kg/m^3 (37^{o}C) (Olivares et al. 2009). A constant uniform inlet fluid velocity profile was applied (v = 100 μm/s or 0.3 mL/min) (Gomes et al. 2003), while no-slip boundary conditions were applied on all scaffold walls and a zero pressure boundary condition was assumed at the outlet. To

distinguish the type of flow (laminar or turbulent), the Reynolds numbers (Re) was calculated according to the following equations.

For the rectangular pore flow:

$$\mathrm{Re} = \frac{\rho v l_1 l_2}{2\mu\left(l_1 + l_2\right)} \tag{2.1}$$

For the hexagonal pore flow:

$$\mathrm{Re} = \frac{\sqrt{3}\rho v l_1}{4\mu} \tag{2.2}$$

where, l_1 and l_2 were the width and length of rectangular pore as shown in Fig. 2(b).

The Reynolds numbers were obtained as 0.0020 and 0.0025 respectively for rectangular pore flow and hexagonal pore flow. Since these values were much smaller than the critical value of 500, the model assumed laminar flow. Finally, the ANSYS CFX solver resolved the model using the finite volume method under the root-mean-square (RMS) residual convergence criteria of 1×10^{-4}.

2.2 Sub-scaffold (cellular level) fluid-structure interaction model

To investigate the mechanical stimulation of osteoblasts under the fluid flow, local two-way fluid-structure interaction models were defined using the ANSYS Multiphysics platform, which coupled the ANSYS CFX solver and ANSYS Structure finite element solver. Specifically we investigated the effect of cell attachment at different locations along the scaffold, by developing three sub-scaffold FSI models representing three different regions (*C*, *M*, *F* in Fig. 2(a)) where the boundary conditions were derived from the global model (described above), since the local pressure and fluid velocity fields were found to vary along the longitudinal direction of global scaffold.

The difference in cell geometry was investigated to account for osteoblasts that attached to the scaffold or bridged scaffold pores. In each sub-scaffold FSI model, we modelled four osteoblasts bridging across the pores and five osteoblasts attaching on the scaffold surfaces (see Fig. 2(b)). The cell geometry reported by Jungreuthmayer et al. (2009) was idealised and altered to incorporate a nucleus and cytoplasm section in the cell model (see Fig. 2(c)). The cell body of attached and bridged cells were idealised as a hemisphere/sphere, respectively, with diameters of 19μm and 15μm. The

heights of cell extensions were 0.75μm and 1.0μm for attached and bridged cells, respectively. Moreover, both the attached and bridged cells had a uniform length of 60μm. In this study, we referred to each individual cell in the sub-scaffold FSI model through a naming convention, e.g. *AC1*, *AC2, BM3, BF4*. Here, *A* and *B* represented attached and bridged osteoblasts and the number *1, 2, 3* and *4* represented different locations within a sub-scaffold (Fig. 2(b)). The letters *C, M* and *F* denoted the three different regions of global scaffold in which the osteoblasts were located, where Region *C* corresponds to a region near the scaffold inlet, Region *M* corresponds to a region in the middle of the scaffold while Region *F* corresponds to a location near the scaffold outlet (Fig. 2(a)). All the osteoblasts were meshed using the Hex Dominant method, which generated 86,000 elements and 70,500 elements for attached and bridged osteoblasts, respectively.

We assumed that the cell cytoplasm and nucleus were isotropic and compressible materials (McCoy et al. 2012; Sugawara et al. 2008; Verbruggen et al. 2012). For the cytoplasm, a Young's modulus (E_{cyto}) and a Poisson's ratio (v) of 4.47kPa and 0.4 were assumed, while the Young's modulus (E_{nucl}) of nucleus was 17.88kPa and Poisson's ratio was 0.4 (Vaughan et al. 2013). It was assumed that the cell body and scaffold were perfectly adhered, which prevented fluid penetrating the cell-scaffold interface. The cell body surface was set as the fluid-solid interface, where the media generated the WSS and fluid pressure as the load to cells. The solid model of osteoblasts was resolved by an iterative solver using FE method.

The fluid properties in local FSI model were the same as those in the global CFD model described above. The inlet fluid velocity profile (matrix **v**) of the sub-scaffold was the local fluid velocity profile predicted by the global CFD model. As shown in Fig. 3(c), six side faces of the fluid domain assumed a symmetry condition, which inhibited out-of-plane flow. The outlet boundary condition assumed as a static pressure ($\boldsymbol{p_1}$), which was derived from the results of the global CFD model (see Fig. 3(c)). The cell membrane formed the fluid-solid interface between the CFD and FE domains and this two-way FSI analysis followed a staggered iteration approach, whereby the fluid equations were solved and the resulting fluid stress tensor acting at any fluid-solid interfaces (in this case the cell membranes) is applied as the boundary condition on the solid domain, where resulting deformations are relayed back to the fluid domain and the solution continues through further iterations

until a convergence criteria is reached. The fluid domain was meshed by a Tetrahedron method with a patch confirming algorithm. Additionally, the mesh on the fluid-solid interface was refined with an element size of 0.2μm. A total of 748,391 elements and 1,106,574 elements discretised the attached and bridged osteoblasts. Finally, the model was resolved in steady state by ANSYS CFX solver under the RMS residual convergence criteria of 1.0×10^{-4}.

2.3 Mechanical compression model

As compression of the scaffold would elicit fluid flow within the fluid filled material, a two-way FSI model was developed based on the global scaffold to determine the WSS and fluid velocity within the scaffold. Olivares et al. (2009) suggest a uniaxial compression with the strain of 0.5% favourable for bone cell differentiation. So, in the solid domain, a time-dependent uniaxial compressive strain (0-0.5%, 1Hz) was applied to the scaffold as shown in Fig. 4(a). The scaffold surfaces were defined as the solid-fluid interfaces, and the scaffold was constrained by frictionless support on the bottom and side surfaces. The entire solid domain was meshed by Hex Dominant method with 14,553 elements, and solved in transient state by FE approach. In the fluid domain, the top and bottom surfaces were assumed as non-slip walls. Similar with the FSI model in Section 2.2, this FSI model also followed a staggered iteration approach, whereby the fluid equations were solved and the fluid shear was computed on the interface between fluid and scaffold. The fluid domain was meshed by a Tetrahedron method with a patch confirming algorithm, resulting in 2,288,900 elements, and resolved in transient state by ANSYS CFX solver under the RMS residual convergence criteria of 1.0×10^{-4}. As shown in Fig. 5, the maximum WSS and fluid velocity caused by compression (0.5% strain) were 0.56mPa and 20μ/s, respectively. Compared to the WSS and fluid velocity by fluid perfusion, the influence of the fluid flow in compression (0.5% strain) could be ignored. Consequently, a finite element (FE) method was employed to determine the stimulation received by attached and bridged cells in scaffold under mechanical compression. The bottom face and six side faces of the sub-scaffold were defined as the frictionless support boundaries as shown in Fig. 4(b). A Hex Dominant method was employed for meshing the sub-scaffold with osteoblasts bridged and attached in it, and 233,978 elements were

generated for the sub-scaffold and cells. Finally, the strains in osteoblasts were computed by ANSYS Structural solver.

3. Results

3.1 Global computational dynamics model

The global CFD model was used to calculate the WSS, pressure and fluid velocity within the scaffold under perfusion fluid flow (v=100μm/s), which informed the boundary conditions for the sub-scaffold (cell level) model. Fig. 3 (a, b) showed the pressure and fluid velocity distribution within the global scaffold. The pressure decreased from 0.95Pa to 0Pa along the longitudinal direction from the inlet to the outlet. Sub-scaffold models were located at three different longitudinal regions, *C*, *M*, and *F*, and at these locations the maximum fluid velocity occurred in the centre of the scaffold channel, as shown in Fig. 6a. Here, the maximum fluid velocities at Region *C*, *M* and *F* were 411μm/s, 393μm/s and 391μm/s, respectively. Fig. 7a shows the percentage of the scaffold surface areas experiencing different levels of WSS indicative for bone cell differentiation (0.1mPa - 10mPa), and cartilage differentiation (10 - 30mPa) (Olivares, et al. 2009; Prendergast, et al. 1997). The results of the global model predicted that 75.4% and 24.4% of total scaffold surface area were exposed to levels of WSS sufficient to stimulate bone and cartilage differentiation, respectively.

3.2 Sub-scaffold (cellular level) fluid-structure interaction model

Figure 6 (a-c) shows the fluid velocity distribution at three different cross-sectional layers inside the sub-scaffold unit. As shown in Fig. 6 (e), the fluid velocity peaked in the central region of the sub-scaffold, and from Layer-1 to Layer-3 the maximum velocity decreased from 393μm/s to 245μm/s for the sub-scaffold model at Region *M* for example, where the effective area of the flow region increases due to the scaffold design. On the symmetric boundary locations (e.g. Position **A** and **D** in Fig. 6(c)), fluid velocities were much lower than the central region.

3.2.1 Influence of the longitudinal regions (C, M, and F) on the wall shear stress of osteoblasts

Figure 7(b) showed the maximum WSS on the osteoblasts that were analysed under the applied boundary conditions from the global CFD model, which was shown to vary within the range from

25mPa to 254mPa, depending on their location within the sub-scaffold. However, it was notable that osteoblasts in each of the different regions of the global scaffold (i.e. Regions *C*, *M* and *F*) received almost identical levels of stimulation, indicating that variation of cells in the longitudinal direction did not alter the maximum WSS imparted on the cells.

3.2.2 Influence of the locations within the sub-scaffold on the wall shear stress of osteoblasts

Variation of the cell locations within the sub-scaffold (*A1-A5* and *B1-B4*) altered the maximum WSS experienced by the osteoblasts as shown in Fig. 7(b). The average value of the maximum WSS on all of the attached osteoblasts and bridged osteoblasts was 50.8mPa and 119.9mPa, respectively. Fig. 7(c, d) showed that the maximum WSS on osteoblasts (τ_{max}) was amplified in the interior of the scaffold compared to the maximum shear stress at the scaffold surface (τ_0). Specifically, osteoblasts at location *A3* showed approximately a five-fold increase of maximum WSS, compared to the maximum scaffold WSS at this location (i.e. $\tau_{max}=5\times\tau_0$). Osteoblasts at locations *A1* and *A2* showed approximately a two-fold increase of WSS, compared to the maximum scaffold WSS at those locations (i.e. $\tau_{max}=2\times\tau_0$), while osteoblasts at locations *A4*, *A5*, *B1*, *B2*, *B3* and *B4* showed approximately a four-fold increase on the maximum scaffold WSS (i.e. $\tau_{max}=4\times\tau_0$).

3.2.3 Influence of longitudinal regions (C, M and F) on the strain of osteoblasts

The influence of longitudinal locations on strain distribution in the osteoblasts was shown in Fig. 8. As depicted in Fig. 8(a, b), the attached osteoblasts in different longitudinal regions (*C*, *M* and *F*) exhibited variation with regard to the strain experienced within the cytoplasm, but no significant variation on the strain in nucleus of attached osteoblasts was observed. No significant difference in strain for bridged osteoblasts in different longitudinal regions was observed. Furthermore, the bridged osteoblasts exhibited much larger strain magnitudes compared to the attached osteoblasts. For attached and bridged osteoblasts, the maximum strains were 240με and 107,100με, respectively, and in both cases were concentrated at the edges of cells that connected to the scaffold surface. Meanwhile, very small strains were observed in the nucleus, 3.6με and 8με for both attached and bridged osteoblasts.

3.2.4 Influence of the locations within the sub-scaffold on the strain of osteoblasts

Figure 9 showed the elastic equivalent strain in the osteoblasts at different locations within the sub-scaffold. For the attached osteoblasts, the maximum strain in the cell extension was higher in *AC5* (397με) than those in *AC1* (100με) and *AC3* (200με*)*. For bridged osteoblasts, the *BC2* cell showed the highest strain in the cell extension (177,200με) compared to the cells in other locations. For the attached osteoblasts, the strain was amplified at the edges of cells that attached to the scaffold surfaces and the end of the cell extensions. For the bridged osteoblasts, the strain was not only concentrated at the connection between cell extensions and the scaffold surface, but also at the connection between the cell bodies and cell extensions. The maximum strains on attached and bridged osteoblasts were 397με and 177,200με, respectively. For the nucleus in both attached and bridged osteoblasts, the strain did not change with the variation of location, and were almost equally distributed with the values of 2με and 65με, respectively.

3.3 Mechanical compression model

The compressive strain distribution in scaffold and osteoblasts was depicted in Fig. 10. As the scaffold showed symmetric strain distribution in the longitudinal direction, we investigated the represented cells of *B3*, *B4*, *A1*, *A3* and *A5*. The cells of *B3*, *A1* and *A5* received very small strain (<1με), which is the same with the strain on the surrounding scaffold surfaces. The Cell *B4* showed the maximum strain of 10,000με, which occurred at the connections between extensions and scaffold surfaces, while the Cell *A3* exhibited the maximum strain of 22,600με that happened not only at the connections between cell and scaffold surfaces but also the junctions between extensions and cell body. In cells extensions of both Cells *B4* and *A3*, the strain was equally distributed with a value of 6,000με.

4. Discussion

In this study, the mechanical stimulation on osteoblasts seeded in a TE scaffold was determined by means of a two-way multiscale FSI and FE computational approach. Importantly, the local sub-scaffold FSI models presented here allowed for an accurate transition between the global scaffold flow conditions and their resulting effect on local cellular deformation in the sub-scaffold FSI model.

This allowed for accurate resolution of local flow fields and WSS profiles in the vicinity of osteoblast cells and our predictions highlighted that WSS imparted on cell membranes could undergo significant amplification (in some cases five-fold), when compared to WSS acting on the scaffold in the same location. The results also showed that (i) for stimulation by flow perfusion: bridged cells were more highly stimulated than attached cells, similar to (Jungreuthmayer *et al.* 2009; McCoy et al. 2012); (ii) for stimulation by compression: the attached cells received more stimulation than the bridged cells. We predicted that the magnitude of stimulation to these bridged cells in fluid flow was similar throughout the longitudinal direction of the scaffold, however, showed some degree of variation depending on their location within the sub-scaffold unit cell, with higher magnitudes of stimulation evident in the central region of the sub-scaffold unit cell. Within the local FSI model, we also predicted low flow areas and a certain amount of recirculation in the periphery of the unit cell that resulted in reduced cell stimulation in these areas and could have certain implications for nutrient transport through the scaffold.

One of the main potential limitations in this study was the use of an idealised model to represent the osteoblast geometry, which might not fully represent the cell geometries that would be seen in TE scaffolds *in vitro*. However studies incorporating osteoblast geometries, for e.g. derived from confocal microscopy imaging, would require significant local mesh refinement to accurately resolve all geometric features, especially at the interfaces between cells and fluid where a particular refined mesh was required to solve the pressure and velocity fields, and as such would be computationally challenging. Secondly, the study only considers a single scaffold that had a repeating hexagonal unit cell architecture. It has been shown previously that the chosen scaffold architecture affects fluid flow fields within the scaffold (Olivares, et al. 2009), which would certainly affect subsequent cellular deformation. However, the focus of this paper was to outline a multiscale framework that allowed a suitable prediction of scaffold level forces to cell level deformations. Future studies will include different geometries and focus on the combined effects of porosity and pore size on cell level stimulation using the multiscale framework developed herein. These parameters could have important implications as it has been previously suggested that pore size is a controlling parameter in determining the relative density of bridged and attached cells within the scaffold

(Jungreuthmayer et al. 2009). Thirdly, to simplify the model, we only considered a steady-state solution of fluid flow fields and passive behaviour of osteoblast cell, where the constitutive model was assumed to isotropic and linearly elastic. The assumption of linear isotropy by Verbruggen et al. (2012; 2013) and Blecha et al. (2010) have shown sufficient accuracy to describe cell behaviour for steady-state analysis, due to the small strains involved in the analysis.

The key findings of this study have highlighted significant amplification of WSS at cell membranes compared to the scaffold surfaces. Computational fluid dynamics (CFD) models have characterised fluid flow within scaffolds and have estimated that a wall shear stress (WSS) of 0.1mPa - 10mPa on the scaffold surfaces was favourable for bone cell differentiation (Olivares et al. 2009; Prendergast, et al. 1997), while WSS of 100mPa was estimated to correlate to the enhancement of osteoblast differentiation and proliferation capacity within a cell-seeded scaffold (Ban et al. 2011; Bancroft et al. 2002). Our results in Fig. 7(a) showed that 75.4% of scaffold surface had a WSS of 0.1mPa - 10mPa, which would indicate bone cell differentiation at these locations. In addition, a study by Li et al. (2009) suggested that a scaffold-level WSS in the range of 5mPa – 15mPa could increase the mineralisation and accelerate osteogenic differentiation of MSCs. Correlated to the results in our study, we found that 66.2% of scaffold surface area experienced the WSS between 5mPa and 15mPa, which indicated that osteogenic differentiation of MSCs would be enhanced in these areas. More importantly, due to the high resolution of our local sub-scaffold FSI model, it was shown that the WSS was amplified significantly at the cell level when compared to the predicted WSS from the global model, with certain cases exhibiting a five-fold increase. Interestingly, similar cell level amplification effects of WSS have been observed for 2D cell perfusion systems (Anderson et al. 2006; Vaughan et al. 2013). However, in 2D cell perfusion systems, the WSS magnitudes to stimulate a biochemical response of cells in osteogenic and chondrogenic differentiation were much higher than the levels of WSS in our study. For example, Yourek et al. (2010) and Juhasz et al. (2014) found that the WSSs of 900mPa and 5,000mPa could enhance osteogenic and chondrogenic differentiation, respectively, which were significantly higher than the WSS in our study. However, a recent study also found that fluid pressure dominated the mechanical stimulation of bone cells in parallel plate flow chambers more so than shear stress (Vaughan et al. 2013) and as such the higher levels of WSS

reported for osteogenic differentiation in 2D cell perfusion systems may be confounded by the pressure in each system, which has not been widely characterised or reported.

In Fig. 7(b), osteoblast cells at the location of *A1 (Region C), A2 – A5, B1, B3 (Region M, F) and B4* experienced WSS levels lower than 100mPa, which might indicate that ALP production and osteoblastic differentiation of these cells would be enhanced, based on previous experimental studies of osteoblasts in 3D scaffold under a flow rate of 3mL/min (Bancroft et al. 2002). However, this study noted that the shear stress might exceed of 200mPa after cells produce an extracellular matrix, which would decrease the scaffold porosity. It has also been shown that WSS of 10 – 30mPa can induce osteogenic differentiation of MSCs, whose ALP activity and calcium deposition might significantly increase (Sikavitsas et al. 2003) and cells at locations of *A3, A4* and *A5* experience stresses within this range. In addition, Seliktar et al. (2002) found that shear stresses in the range of 100mPa – 5,000mPa could induce and promote chondrogenic differentiation of stem cells in a 3D scaffold. In this study we predicted that cells at locations *A1, B2* and *B3* (Region *C*) experienced shear stresses within this range and as such might be stimulated to undergo chondrogenic differentiation.

Furthermore, this study found that bridged cells experienced much higher stimulation levels than attached cells in the fluid flow, similar to (Jungreuthmayer et al. 2009; McCoy et al. 2012). Interestingly, bridged cells underwent similar magnitudes of stimulation irrespective of their longitudinal positions in the global scaffold (see Fig. 8). However, the magnitude of stimulation did depend upon on their local position in the sub-scaffold model. In particular, cells located in the central region of the sub-scaffold model experienced highest levels of stimulation due to their exposure to higher fluid velocities, and subsequent shear stresses in these regions. For these bridged cells, our models predicted that it was at the cellular extensions (which form the attachment with the scaffold) that cells experience much higher levels of stimulation (177,200με) compared to the cell body or nucleus regions. Interestingly, an *in vitro* study on osteocyte cells in 2D culture (Adachi et al. 2009) has shown that osteocyte cell processes are much more mechanosensitive than the cell body. Importantly, our models predicted that bridged cells within the scaffold experienced strain levels exceeding 10,000με, which was believed to be the threshold of mechanical strain required to elicit an osteogenic response from bone cells under 2D substrate stretching *in vitro* (You et al. 2000). Also,

these bridged cells showed higher strain levels than recent computational predictions of the mechanical stimuli to bone cells *in vivo*, which were found to be in the range of 23με-26,000με (Verbruggen et al. 2013). In contrast it was found that the attached cells received minimal amounts of strain stimulation, much less than the 10,000με threshold thought to be responsible for osteogenic responses (You et al. 2000), indicating that attached cells might not play any role in bone forming activity under the applied fluid flow stimulus.

It should be noted that predictions of WSS acting on attached cells were only slightly smaller than those predicted on bridged cells implying that both cell types were subject to similar shear stress stimulation from the surrounding fluid field. The vast differences in strain magnitudes were down to the much smaller relative area of cell-scaffold attachment present on bridged cells. A previous statistical study showed that within a scaffold, which had an average pore size of 140μm, 75% of the cells were bridged across the pore of scaffold and 25% of the cells were attached on the scaffold surface (Freyman et al. 2001). Together with the results of the current study, we propose that bone formation in tissue engineered scaffolds might be dictated by bridged cells as these cells appeared to receive much higher levels of stimulation than attached cells in a perfusion system. Similar to the findings of Jungreuthmayer et al. (2009), this would have important implications for scaffold design as different pore sizes could affect the likelihood of cells either bridging or attaching directly to the scaffold during the cell seeding process.

This study also showed that the sub-scaffold FSI model had certain regions with very low flow velocities and even some areas of recirculation. These occurred in peripheral regions of the unit cell and were likely a result of the regular cross section of the scaffold strut, which caused separation of the flow and resulting recirculation (Fig. 6(d)). In these local regions, reduced cell stimulation was evident and such areas could potentially result in reduced nutrient transport through the scaffold, which could impede osteogenic differentiation in an *in vitro* environment. The methods developed here could be implemented for numerical scaffold design optimisation to avoid the occurrence of such regions in TE scaffolds. The results shown here highlighted that cells located in more central regions of the unit cell sub-scaffold geometry received higher levels of stimulation.

In addition, the study of stimulation by mechanical compression (0-0.5% strain; 1Hz) revealed that the attached cells were more highly stimulated than the bridged cells. Moreover, some cells (i.e. *B1*, *B4* and *A3*) could experience the strain in excess of the threshold for osteogenic response (10,000με) (You et al. 2000). Therefore a change in pore size might affect the amount of bridged cells and attached cells, and thereby alter the stimulation received by the cells within the scaffold. Furthermore, the results of this study show that, for mechanical stimulation by compression at large strain magnitudes or high frequency, the influence of fluid flow caused by compression is significant and should be considered as an additional stimulus to the cells within a fluid filled porous TE scaffold.

Finally, after comparing the flow perfusion system (inlet fluid velocity of 100μm/s) to the mechanical compression system (applied strain of 0.5%), we suggest that a combination of flow perfusion and mechanical compression is preferable for enhancing bone cell differentiation. Specifically, we predicted that more bridged osteoblasts received strains in excess of the threshold of osteogenic differentiation (10,000με) in the perfusion system, whereas more attached cells experienced strain over this threshold in the compression system. On the other hand, the mechanical stimulation by compression had some limitations, compared to flow perfusion system. Firstly, the WSS on cells stimulated in mechanical compression system was so low that it could be ignored, particularly when compared to the WSS level in perfusion systems. From the perspective of nutrient transport, as the fluid velocity was much larger in the perfusion system than that in the compression system, the culture medium would be more greatly forced to distribute through the pores of scaffold, thereby enhancing the nutrient transport and improving the mass transfer rate not only at the strut periphery but also within the internal pores. Therefore, a combination of flow perfusion and mechanical compression may compensate for the limitations of each other.

5 Conclusions

In this study, we developed a novel multiscale CFD and FSI model to determine the mechanical stimulation of osteoblast cells in TE scaffold under fluid flow, and a FE model to show the stimulation of osteoblast cells in TE scaffold under mechanical compression. The WSS, fluid velocity

and pressure in the global scaffold were characterised by the global CFD model, and the mechanical stimulation of osteoblasts was determined by implementing a sub-scaffold (cellular level) FSI model, with boundary conditions derived from CFD model. We predicted that there was significant amplification of WSS on cell membranes in the sub-scaffold model, when compared to the WSS acting on the scaffold surface in similar locations (in some cases a five-fold increase). It was shown that bridged cells within the TE scaffold were highly stimulated, whereas attached cells received minimal levels of stimulation. Interestingly, for stimulation by mechanical compression, the FE model revealed that attached cells experienced higher stimulation than bridged cells. For stimulation by perfusion, cellular stimulation tended to be at a maximum within the central channel of the sub-scaffold model. The study also highlighted that in peripheral regions of the sub-scaffold unit cell experience low fluid velocities and relatively low levels of stimulation. Finally, we propose that a combination of flow perfusion and mechanical compression is preferable for osteogenic differentiation, by means of stimulating both attached and bridged cells in excess of the strain threshold for osteogenic differentiation (10,000με).

Acknowledgement

The authors would like to acknowledge the funding provided by the European Research Council (ERC) under grant number 258992 (BONEMECHBIO). In addition, the first author wishes to express his gratitude to Dr. S. W. Verbruggen (Biomedical Engineering, National University of Ireland, Galway) for his help with model generation.

References:

Adachi T, Aonuma Y, Tanaka M, Takano-Yamamoto T, Kamioka H (2009) Calcium response in single osteocytes to locally applied mechanical stimulus: differences in cell process and cell body. J Biomech 42(12): 1989-95. doi: 10.1016/j.jbiomech.2009.04.034

Anderson EJ, Falls TD, Sorkin AM, Knothe Tate ML (2006) The imperative for controlled mechanical stresses in unraveling cellular mechanisms of mechanotransduction. Biomed Eng Online 5:27. doi: 10.1186/1475-925X-5-27

Bacabac RG, Smit TH, Mullender MG, Dijcks SJ, Van Loon JJWA, Klein-Nulend J (2004) Nitric oxide production by bone cells is fluid shear stress rate dependent. Biochem Biophys Res Commun 315(4): 823-829. doi: 10.1016/j.bbrc.2004.01.138

Ban Y, Wu YY, Yu T, Geng N, Wang YY, Liu XG, Gong P (2011) Response of osteoblasts to low fluid shear stress is time dependent. Tissue Cell 43(5): 311-7. doi: 10.1016/j.tice.2011.06.003

Bancroft GN, Sikavitsas VI, van den Dolder J, Sheffield TL, Ambrose CG, Jansen JA, Mikos AG (2002) Fluid flow increases mineralized matrix deposition in 3D perfusion culture of marrow stromal osteoblasts in a dose-dependent manner. Proc Natl Acad Sci U S A 99(20): 12600-5. doi: 10.1073/pnas.202296599

Blecha LD, Rakotomanana L, Razafimahery F, Terrier A, Pioletti DP (2010) Mechanical interaction between cells and fluid for bone tissue engineering scaffold: modulation of the interfacial shear stress. J Biomech 43(5): 933-7. doi: 10.1016/j.jbiomech.2009.11.004

Birmingham E, Grogan JA, Niebur GL, McNamara LM, McHugh PE (2013) Computational modelling of the mechanics of trabecular bone and marrow using fluid structure interaction techniques. Ann Biomed Eng 41(4): 814-826. doi: 10.1007/s10439-012-0714-1

Byrne DP, Lacroix D, Planell JA, Kelly DJ, Prendergast PJ (2007) Simulation of tissue differentiation in a scaffold as a function of porosity, Young's modulus and dissolution rate: Application of mechanobiological models in tissue engineering. Biomaterials 28(36): 5544-54. doi: 10.1016/j.biomaterials.2007.09.003

Freyman TM, Yannas IV, Pek Y-S, Yokoo R, Gibson LJ (2001) Micromechanics of fibroblast contraction of a collagen-GAG matrix. Exp Cell Res 269(1): 140-53. doi: 10.1006/excr.2001.5302

Goldstein AS, Juarez TM, Helmke D, Gustin MC, Mikos AG (2001) Effect of convection on osteoblastic cell growth and function in biodegradable polymer foam scaffold. Biomaterials 22(11): 1279-88. doi: 10.1016/S0142-9612(00)00280-5

Gomes ME, Sikavitasa VI, Behravesh E, Reis RL, Mikos AG (2003) Effect of flow perfusion on the osteogenic differentiation of bone marrow stromal cells cultured on starch-based three dimensional scaffolds. J Biomed Mater Res A 67(1): 87-95. doi: 10.1002/jbm.a.10075

Jaasma MJ, Plunkett NA, O'Brien FJ (2008) Design and validation of a dynamic flow perfusion bioreactor for use with compliant tissue engineering scaffolds. J Biotechnol 133(4): 490-6. doi: 10.1016/j.jbiotec.2007.11.010

Juhasz T, Matta C, Somogyi C, Katona E, Takacs R, Soha RF, Szabo IA, Cserhati C, Szody R, Karacsonyi Z, Bako E, Gergely P, Zakany R (2014) Mechanical loading stimulates chondrogenesis visa the PKA/CREB-Sox9 and PP2A pathways in chicken micromass cultures. Cell Signal 26(3): 468-82. doi: 10.1016/j.cellsig.2013.12.001

Jungreuthmayer C, Jaasma MJ, Al-Munajjed AA, Zanghellini J, Kelly DJ, O'Brien FJ (2009) Deformation simulation of cells seeded on a collagen-GAG scaffold in a flow perfusion bioreactor using a sequential 3D CFD-elastostatics model. Med Eng Phys 31(4): 420-7. doi: 10.1016/j.medengphy.2008.11.003

Keogh MB, Partap S, Daly JS, O'Brien FJ (2011) Three hours of perfusion culture prior to 28 days of static culture, enhances osteogenesis by human cells in a collagen GAG scaffold. Biotechnol Bioeng 108(5): 1203-10. doi: 10.1002/bit.23032

Kim K, Yeatts A, Dean D, Fisher JP (2010) Stereolithographic bone scaffold design parameters: osteogenic differentiation and signal expression. Tissue Eng Part B Rev 16(5): 523-39. doi: 10.1089/ten.TEB.2010.0171

Klein-Nulend J, van der Plas A, Semeins CM, Ajubi NE, Frangos JA, Nijweide PJ, Burger EH (1995) Sensitivity of osteocytes to biomechanical stress in vitro. FASEB J 9(5): 441-5.

Li D, Tang T, Lu J, Dai K (2009) Effects of flow shear stress and mass transport on the construction of a large-scale tissue-engineered bone in a perfusion bioreactor. Tissue Eng Part A 15(10): 2773-83. doi: 10.1089/ten.TEA.2008.0540

Li M, Liu W, Sun J, Xianyu Y, Wang J, Zhang W, Zheng W, Huang D, Di S, Long YZ, Jiang X (2013) Culturing primary human osteoblasts on electrospum Poly(lactic-co-glycolic acid) and Poly(lactic-co-glycolic acid)/nanohydroxyapatite scaffolds for bone tissue engineering. ACS Appl Mater Interfaces 5(13): 5921-6. doi: 10.1021/am401937m

Liu L, Yu B, Chen J, Tang Z, Zong C, Shen D, Zheng Q, Tong X, Gao C, Wang J (2012) Different effects of intermittent and continuous fluid shear stresses on osteogenic differentiation of human mesenchymal stem cells. Biomech Model Mechanobiol 11(3-4): 391-401. doi: 10.1007/s10237-011-0319-x

Lupu-Haber Y, Pinkas O, Boehm S, Scheper T, Kasper C, Machluf M (2013) Functionalized PLGA-doped zirconium oxide ceramics for bone tissue regeneration. Biomed Microdevices 15(6): 1055-66. doi: 10.1007/s 10544-013-9797-1

Lyons FG, Al-Munajjed AA, Kieran SM, Toner ME, Murphy CM, Duffy GP, O'Brien FJ (2010) The healing of bony defects by cell-free collagen-based scaffolds compared to stem cells-seede tissue engineered constructs. Biomaterials 31(35): 9232-43. doi: 10.1016/j.biomaterials.2010.08.056

McCoy RJ, Jungreuthmayer C, O'Brien FJ (2012) Influence of flow rate and scaffold pore size on cell behaviour during mechanical stimulation in a flow perfusion bioreactor. Biotechnol Bioeng 109(6): 1583-94. doi: 10.1002/bit.24424

Milan JL, Planell JA, Lacroix D (2009) Computational modelling of the mechanical environment of osteogenesis within a polylactic acid-calcium phosphate glass scaffold. Biomaterials 30(25): 4219-26. doi: 10.1016/j.biomaterials.2009.04.026

Olivares AL, Marsal E, Planell JA, Lacroix D (2009) Finite element study of scaffold architecture design and culture conditions for tissue engineering. Biomaterials 30(30): 6142-9. doi: 10.1016/j.biomaterials.2009.07.041

Owan I, Burr DB, Turner CH, Qiu J, Tu J, Onyia JE, Duncan RL (1997) Mechanotransduction in bone: osteoblasts are more responsive to fluid force than mechanical strain. Am J Physiol Cell Physiol 273(3): C810-C815.

Park SH, Park DS, Shin JW, Kang YG, Kim HK, Yoon TR, Shin JW (2012) Scaffolds for bone tissue engineering fabricated from two different materials by the rapid prototyping technique: PCL versus PLGA. J Mater Sci Mater Med 23(11): 2671-8. doi: 10.1007/s10856-012-4738-8

Ryan G, McGarry P, Pandit A, Apatsidis D (2009) Analysis of the mechanical behaviour of a Titanium scaffold with a repeating unit-cell substructure. J Biomed Mater Res B Appl Biomater 90(2): 894-906. doi: 10.1002/jbm.b.31361

Samavedi S, Guelcher SA, Goldstein AS, Whittington AR (2012) Response of bone marrow stromal cells to graded co-electropun scaffolds and its implications for engineering the ligament-bone interface. Biomaterials 33(31): 7727-35. doi: 10.1016/j.biomaterials.2012.07.008

Seliktar D, Dunkelman N, Peterson AE, Schreiber RE, Willoughby J, Naughton GK (2002) Application of shear flow stress to chondrocytes. Google Patents EP1019489 A4.

Sikavitsas VI, Bancroft GN, Lemoine JJ, Liebschner MA, Dauner M, Mikos AG (2005) Flow perfusion enhances the calcified matrix deposition of marrow stromal cells in biodegradable nonwoven fiber meh scaffolds. 33(1): 63-70. doi: 10.1007/s10439-005-8963-x

Sittichockechaiwut A, Scutt AM, Ryan AJ, Bonewald LF, Reilly GC (2009) Use of rapid mineralising osteoblasts and short periods of mechanical loading to accelerate matrix maturation in 3D scaffolds. Bone 44(5): 822-9. doi: 10.1016/j.bone.2008.12.027

Stops AJ, McMahon LA, O'Mahoney D, Prendergast PJ, McHugh PE (2008) A finite element prediction of strain on cells in a highly porous collagen-gycosaminoglycan scaffold. J Biomech Eng 130(6): 061001. doi: 10.1115/1.2979873

Stops AJ, Harison NM, Haugh MG, O'Brien FJ, McHugh PE (2010) Local and regional mechanical characterisation of a collagen-gycosaminoglycan scaffold using high-resolution finite element analysis. J Mech Behav Biomed Mater 3(4): 292-302. doi: 10.1016/j.jmbbm.2009.12.003

Thompson MS, Epari DR, Bieler F, Duda GN (2010) In vitro models for bone mechanobiology: applications in bone regeneration and tissue engineering. Proc Inst Mech Eng H 224(12): 1533-41. doi: 10.1243/09544119JEIM807

Vaughan TJ, Haugh MG, McNamara LM (2013) A fluid-structure interaction model to characterize bone cell stimulation in parallel-plate flow chamber systems, J R Soc Interface 10(81): 20120900. doi: 10.1098/rsif.2012.0900

Verbruggen SW, Vaughan TJ, McNamara LM (2012) Strain amplification in bone mechanobiology: a computational investigation of the in vivo mechanics of osteocytes. J R Soc Interface 9(75): 2735-44. doi: 10.1098/rsif.2012.0286

Verbruggen SW, Vaughan TJ, McNamara LM (2013) Fluid flow in the osteocyte mechanical environment: a fluid-structure interaction approach. Biomech Model Mechanobiol. doi: 10.1007/s10237-013-0487-y

Vozzi G, Corallo C, Carta S, Fortina M, Gattazzo F, Galletti M, Giordano N (2013) Collagen-gelatin-genipin-hydroxyapatite composite scaffolds colonized by human primary osteoblasts are suitable for bone tissue engineering application: In vitro evidences. J Biomed Mater Res A. doi: 10.1002/jbm.a.34823

Westbroek I, Ajubi NE, Alblas MJ, Semeins CM, Klein-Nulend J, Burger EH, Nijweide PJ (2000) Differential stimulation of prostaglandin G/H synthase-2 in osteocytes and other osteogenic cells by pulsating fluid flow. Biochem Biophys Res Commun 268(2): 414-19. doi: 10.1006/bbrc.2000.2154

Xie L, Zhang N, Marsano A, Vunjak-Novakovic G, Zhang Y, Lopez MJ (2013) In vitro mesenchymal trilineage differentiation and extracellular matrix production by adipose and bone marrow derived adult equine multipotent stromal cells on a collagen scaffold. Stem Cell Rev 9(6): 858-72. doi: 10.1007/s12015-013-9456-1

You J, Yellowley CE, Donahue HJ, Zhang Y, Chen Q, Jacobs CR (2000) Substrate deformation levels associated with routine physical activity are less stimulatory to bone cells relative to loading-induced oscillatory fluid flow. J Biomech Eng 122(4): 387-93. doi: 10.1115/1.1287161

Yourek G, McCormick SM, Mao JJ, Reilly GC (2010) Shear stress induces osteogenic differentiation of human mesenchymal stem cells. Regen Med 5(5): 713-24. doi: 10.2217/rme.10.60

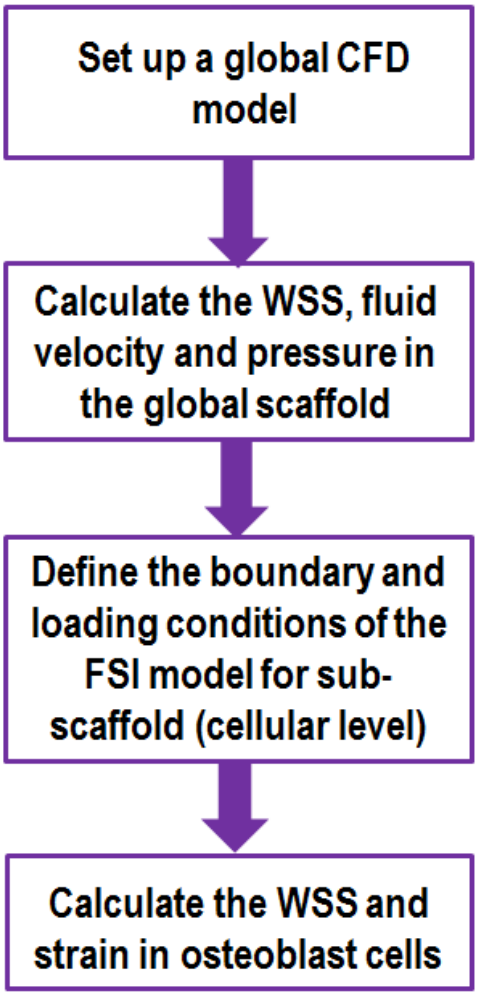

Fig. 1 Flowchart of the multiscale modelling approach.

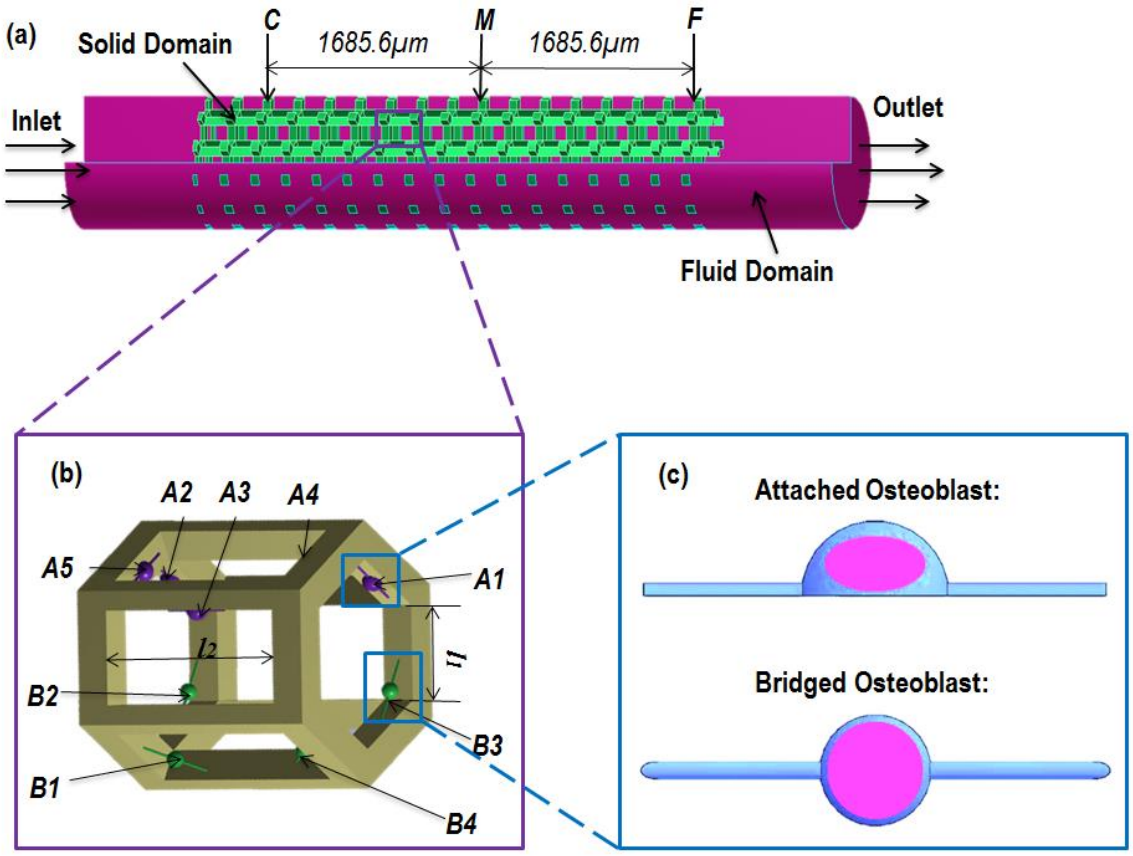

Fig. 2 (**a**) Computational fluid dynamics model showing the fluid domain (pink) and the scaffold solid domain (green), (**b**) sub-scaffold (cellular level model) depicting osteoblast cells attached to the scaffold surface in different locations (*A1*, *A2*, *A3*, *A4*, *B1*, *B2*, *B3*, *B4*, *B5*), (**c**) geometries of bridged and attached osteoblasts.

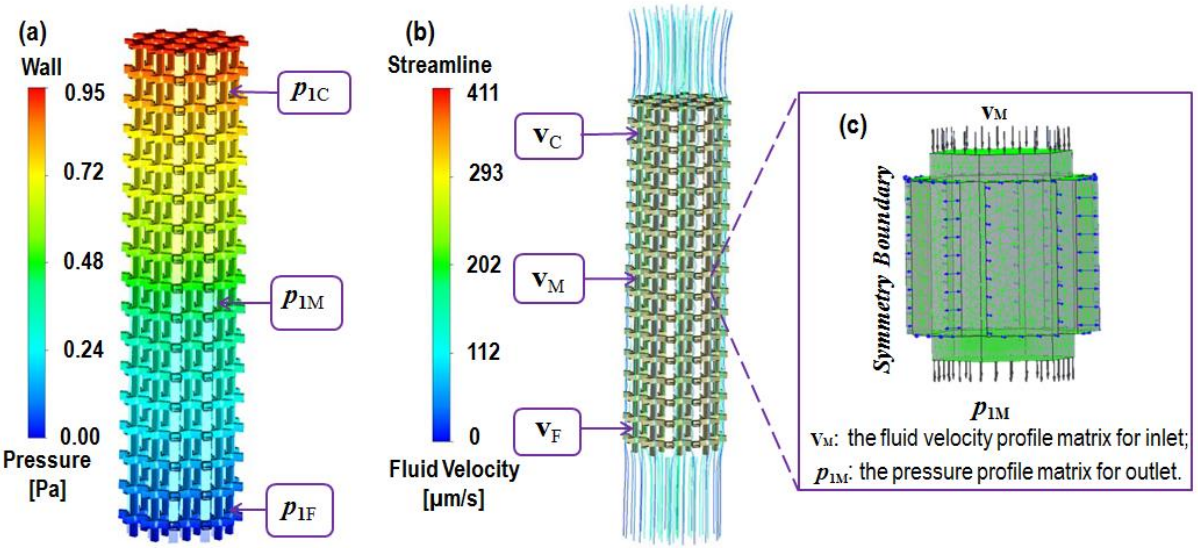

Fig. 3 (**a**) Pressure; (**b**) fluid velocity distribution in global computational fluid dynamics model; (**c**) boundary loading of local fluid structure interaction model.

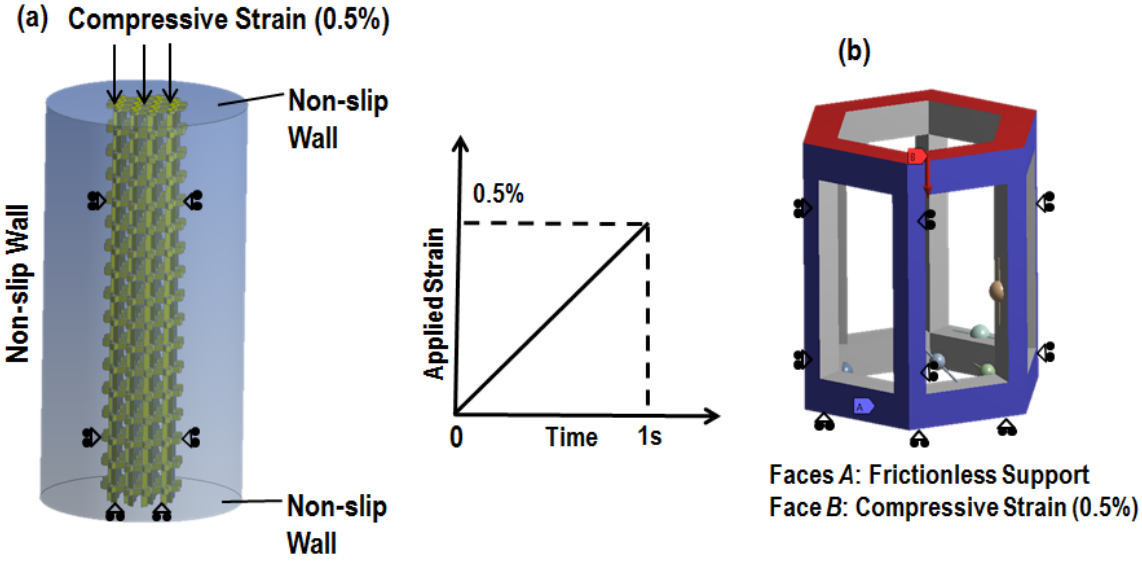

Fig. 4 The boundary conditions of: (**a**) fluid structure interaction model for the global scaffold and (**b**) finite element model for the sub-scaffold under mechanical compression.

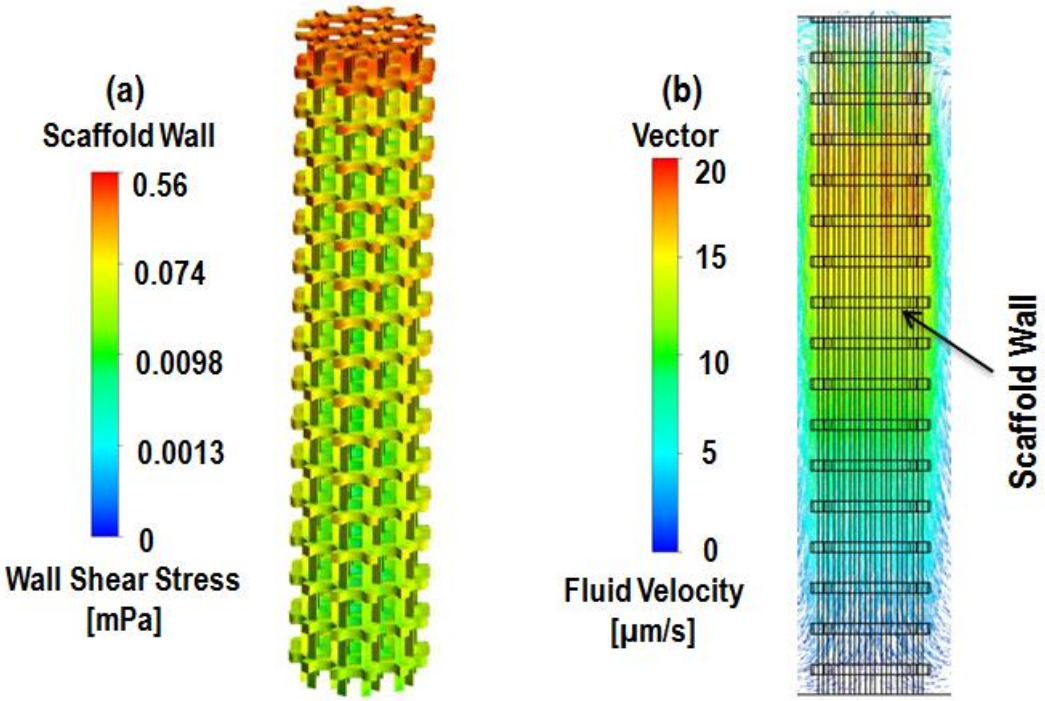

Fig. 5 (**a**) Wall shear stress and (**d**) fluid velocity distribution within the scaffold under compression (0-0.5%, 1Hz).

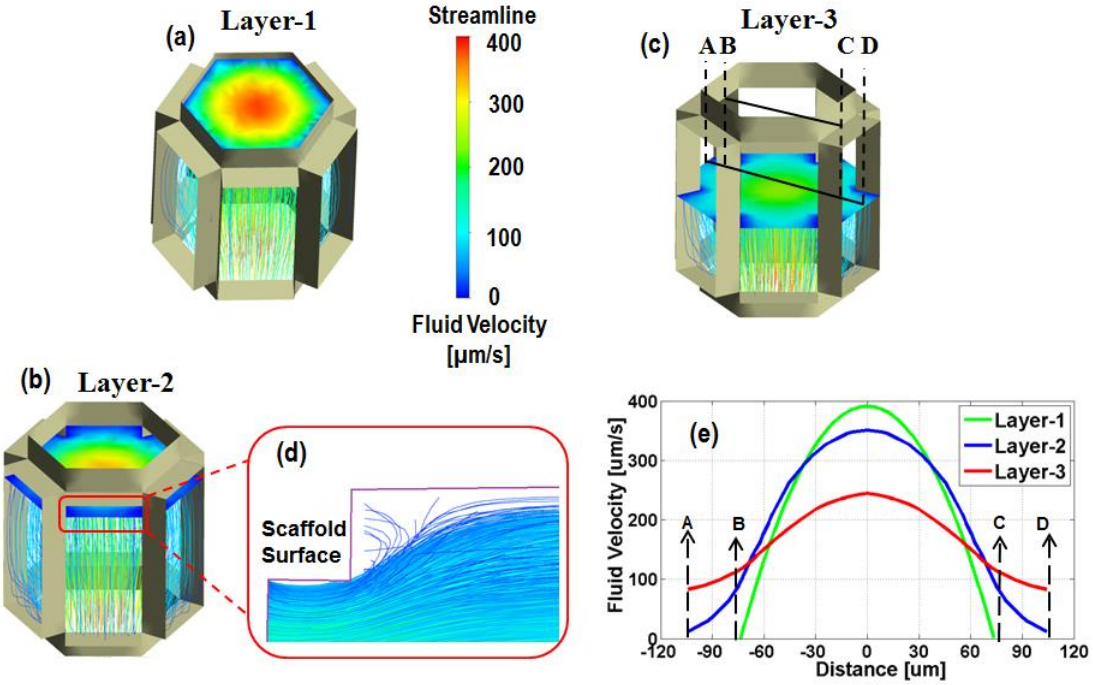

Fig. 6 (**a-c**) Fluid velocity distribution in a sub-scaffold (from Region *M*) at three different layers; (**d**) the region with fluid flow recirculation; (**e**) fluid velocity profiles at three different layers in a sub-scaffold.

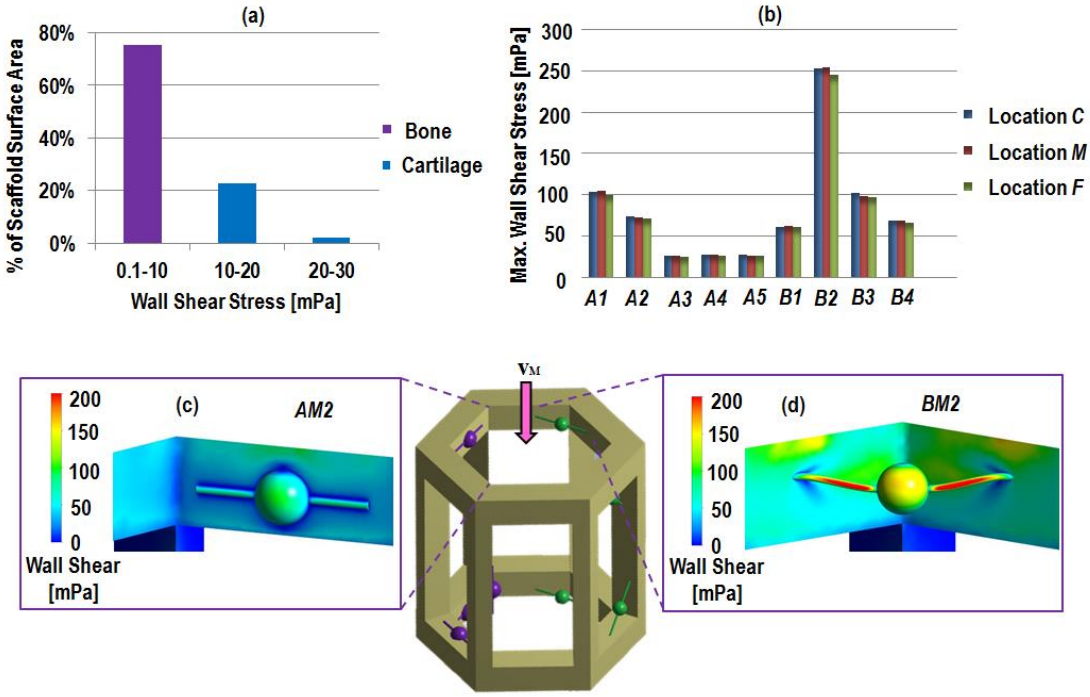

Fig. 7 (**a**) Percentage of global scaffold surface area that undergoes different wall shear stress ranges; (**b**) maximum wall shear stress on every cell; (**c**) wall shear stress distribution on the cell of *AM2* and its surrounding scaffold surface; (**d**) wall shear stress distribution on the cell of *BM2* and its surrounding scaffold surface.

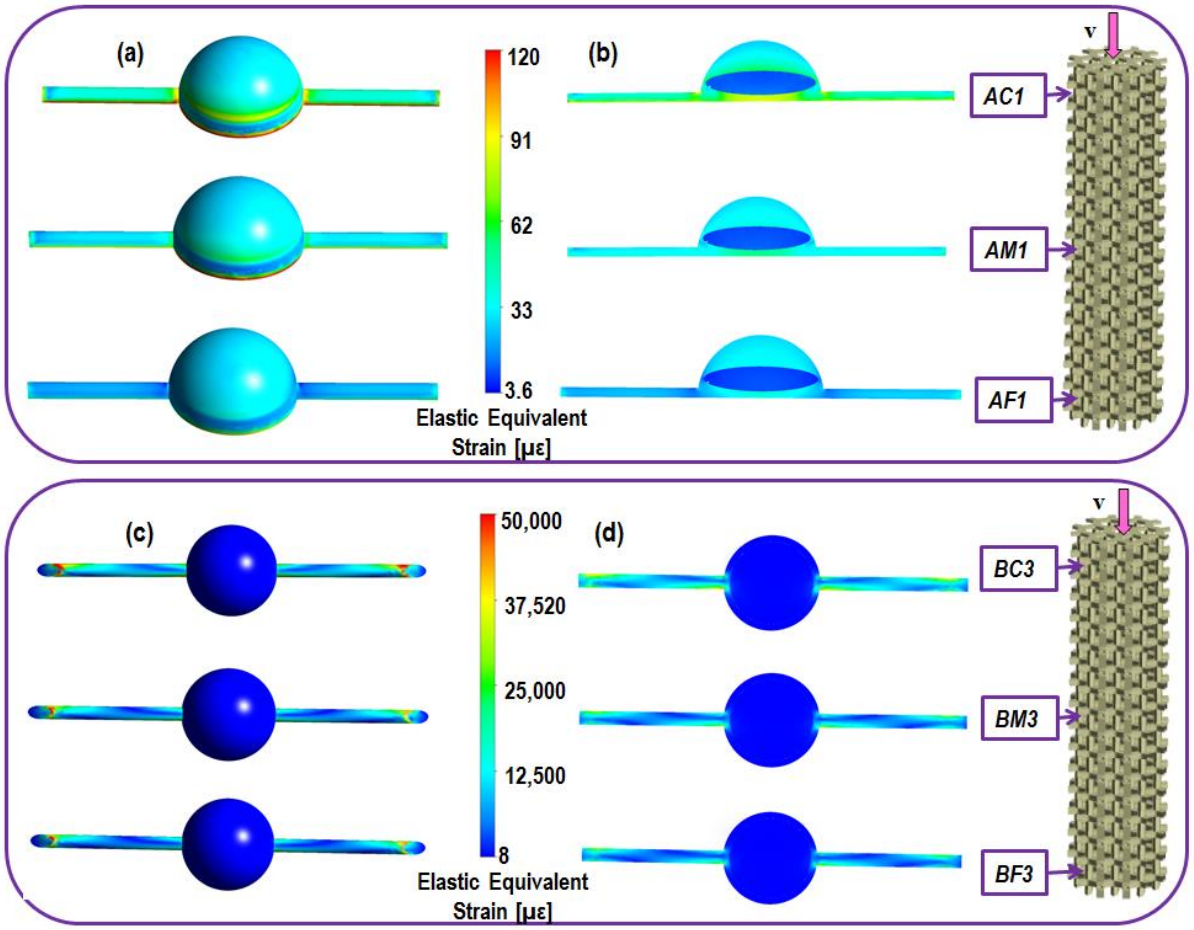

Fig. 8 Influence of different longitudinal regions (*C*, *M* and *F*) within global scaffold on strain of: (**a**) entire attached osteoblasts; (**b**) cytoplasm and nucleus of attached osteoblasts (cross-sectional view); (**c**) entire bridged osteoblasts; (**d**) cytoplasm and nucleus of bridged osteoblasts (cross-sectional view).

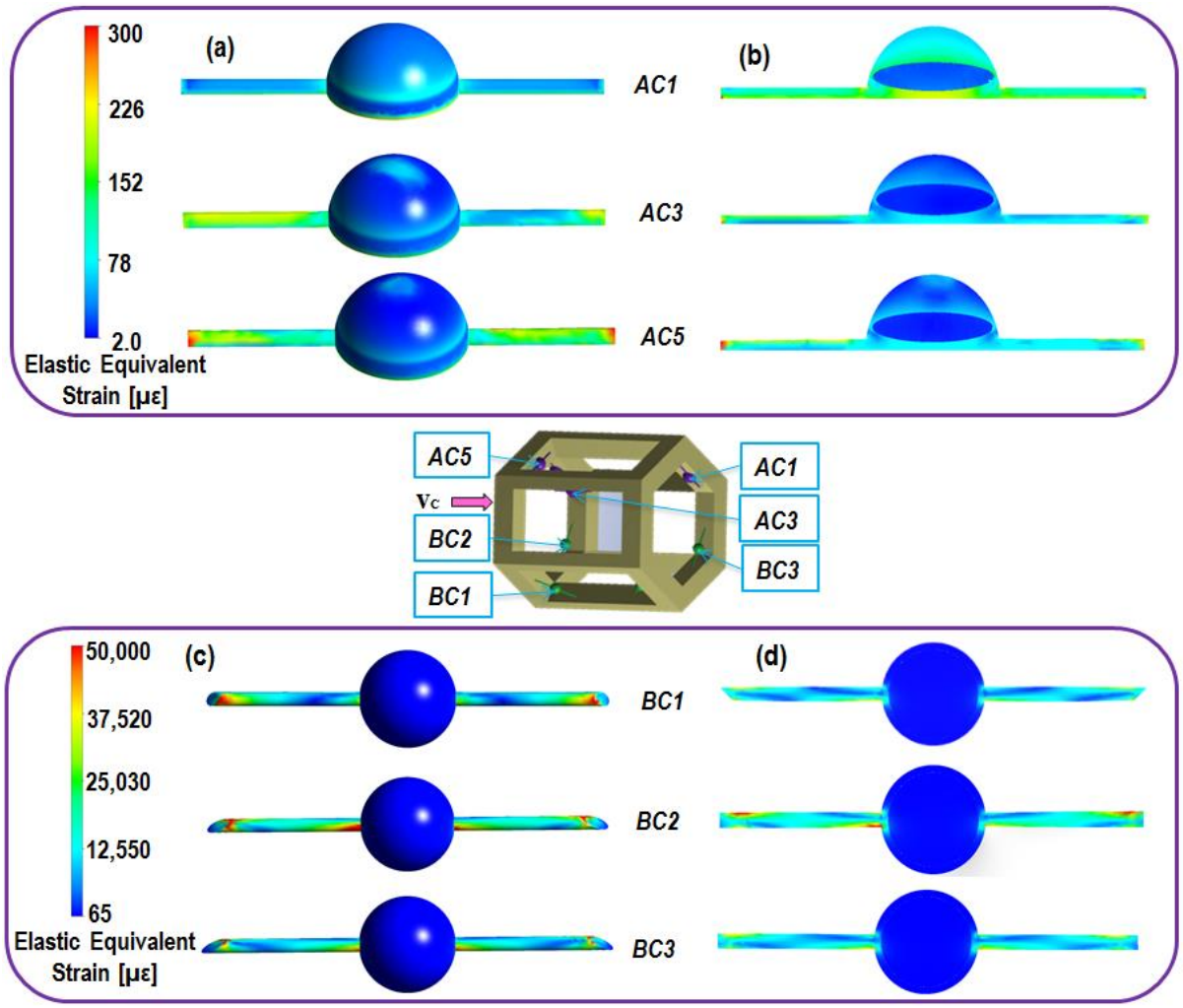

Fig. 9 Influence of different locations within sub-scaffold on the strain of: (**a**) entire attached osteoblasts; (**b**) cytoplasm and nucleus of attached osteoblasts (cross-sectional view); (**c**) entire bridged osteoblasts; (**d**) cytoplasm and nucleus of bridged osteoblasts (cross-sectional view).

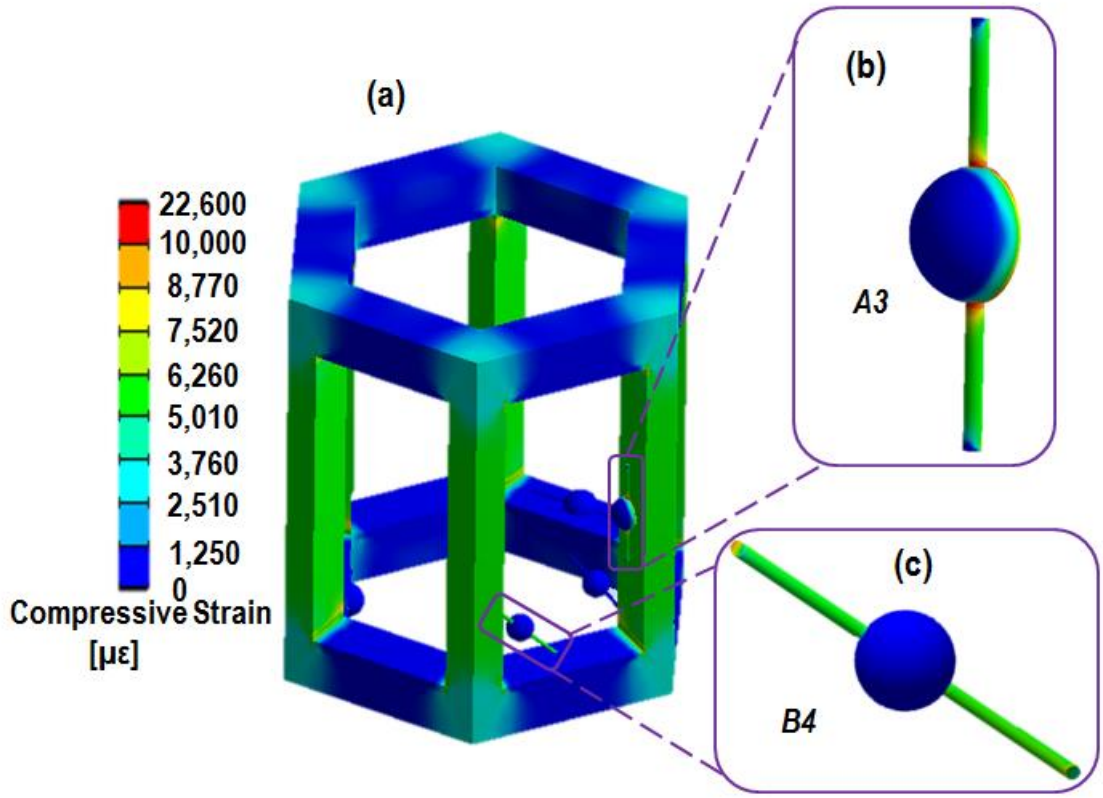

Fig. 10 (**a**) Compressive strain distribution in a sub-scaffold and osteoblasts; compressive strain distribution in: (**b**) the attached cells of *A3* and (**c**) bridged cell of *B4*.